

HYPERON-QUARK MIXED PHASE IN DENSE MATTER

TOSHIKI MARUYAMA* and SATOSHI CHIBA

*Advanced Science Research Center, Japan Atomic Energy Agency,
Tokai, Ibaraki 319-1195, Japan*

**E-mail: maruyama.toshiki@jaea.go.jp*

HANS-JOSEF SCHULZE

INFN Sezione di Catania, Via Santa Sofia 64, Catania I-95123, Italy

TOSHITAKA TATSUMI

Department of Physics, Kyoto University, Kyoto 606-8502, Japan

We investigate the properties of the hadron-quark mixed phase in compact stars using a Brueckner-Hartree-Fock framework for hadronic matter and the MIT bag model for quark matter. We find that the equation of state of the mixed phase is similar to that given by the Maxwell construction. The composition of the mixed phase, however, is very different from that of the Maxwell construction; in particular, hyperons are completely suppressed.

Keywords: Neutron star; Mixed phase; Hyperon mixture; Quark matter; Pasta structure

1. Introduction

Matter in neutron stars (NS) has a variety of density and chemical component due to the presence of gravity. At the crust of neutron stars, there exists a region where the density is lower than the normal nuclear density, $\rho_0 \approx 0.17 \text{ fm}^{-3}$ over a couple of hundreds meters. The pressure of such matter is mainly contributed by degenerate electrons, while baryons are clusterized and have little contribution. Due to the gravity pressure and density increase in the inner region (in fact, the density at the center amounts to several times ρ_0). Cold catalyzed matter consists of neutrons and the equal number of protons and electrons under chemical equilibrium. Since the kinetic energy of degenerate electrons is much higher than that of baryons, the electron fraction (or the proton one) decreases with increase of density and thus neutrons become the main component and drip out of the clusters. In this way baryons come to contribute to the pressure as well as electrons. At a certain density, other components such as hyperons and strange mesons may emerge. At even higher density, hadron-quark deconfinement transition may occur and quarks in hadrons are liberated.

It is well known that hyperons appear at several times ρ_0 and lead to a strong

softening of the EOS with a consequent substantial reduction of the maximum neutron star mass. Actually the microscopic Brueckner-Hartree-Fock approach gives much lower masses than current observation values of $\sim 1.4M_\odot$.

On the other hand, the hadron-quark deconfinement transition is believed to occur in hot and/or high-density matter. Taking EOS of quark matter within the MIT bag model, the maximum mass can increase to the Chandrasekhar limit once the deconfinement transition occurs in hyperon matter.^{1,2}

The deconfinement transition from hadron to quark phase may occur as a first-order phase transition. There, a hadron-quark mixed phase should appear, where charge density as well as baryon number density is no more uniform. Owing to the interplay of the Coulomb interaction and the surface tension, the mixed phase can have exotic shapes called pasta structures.³

Generally, the appearance of mixed phase in matter results in a softening of the EOS. The bulk Gibbs calculation (BG) of the mixed phase, without the effects of the Coulomb interaction and surface tension, leads to a broad density region of the mixed phase (MP).⁴ However, if one takes into account the geometrical structures in the mixed phase and applies the Gibbs conditions, one may find that MP is considerably limited and thereby the EOS approaches to the one given by the Maxwell construction (MC).^{3,5,6}

In this report we explore the EOS and the structure of the mixed phase during the hyperon-quark transition, properly taking account of the Gibbs conditions together with the pasta structures.

2. Numerical Calculation

The numerical procedure to determine the EOS and the geometrical structure of the MP is similar to that explained in detail in Ref. 3. We employ a Wigner-Seitz approximation in which the whole space is divided into equivalent Wigner-Seitz cells with a given geometrical symmetry, sphere for three dimension (3D), cylinder for 2D, and slab for 1D. A lump portion made of one phase is embedded in the other phase and thus the quark and hadron phases are spatially separated in each cell. A sharp boundary is assumed between the two phases and the surface energy is taken into account in terms of a surface-tension parameter σ . The energy density of the mixed phase is thus written as

$$\epsilon = \frac{1}{V_W} \left[\int_{V_H} d^3r \epsilon_H(\mathbf{r}) + \int_{V_Q} d^3r \epsilon_Q(\mathbf{r}) + \int_{V_W} d^3r \left(\epsilon_e(\mathbf{r}) + \frac{(\nabla V_C(\mathbf{r}))^2}{8\pi e^2} \right) + \sigma S \right], \quad (1)$$

where the volume of the Wigner-Seitz cell V_W is the sum of those of hadron and quark phases V_H and V_Q , S the quark-hadron interface area. ϵ_H , ϵ_Q and ϵ_e are energy densities of hadrons, quarks and electrons, which are functions of local densities $\rho_a(\mathbf{r})$ ($a = n, p, \Lambda, \Sigma^-, u, d, s, e$). The Coulomb potential V_C is obtained by solving the Poisson equation. For a given density ρ_B , the optimum dimensionality of the cell, the cell size R_W , the lump size R , and the density profile of each component

are searched for to give the minimum energy density. We employ $\sigma = 40 \text{ MeV/fm}^2$ in the present study.

To calculate ϵ_H in the hadron phase, we use the Thomas-Fermi approximation for the kinetic energy density. The potential-energy density is calculated by the nonrelativistic BHF approach¹ based on microscopic NN and NY potentials.

$$\epsilon_H = \sum_{i=n,p,\Lambda,\Sigma^-} \sum_{k < k_F^{(i)}} \left[T_i(k) + \frac{1}{2} U_i(k) \right], \quad (2)$$

$$U_i(k) = \sum_{j=n,p,\Lambda,\Sigma^-} U_i^{(j)}(k) \quad (3)$$

$$U_i^{(j)}(k) = \sum_{k' < k_F^{(j)}} \text{Re} \langle k k' | G_{(ij)(ij)} [E_{(ij)}(k, k')] | k k' \rangle, \quad (4)$$

$$G_{ab}[W] = V_{ab} + \sum_c \sum_{p,p'} V_{ac} | p p' \rangle \frac{Q_c}{W - E_c + i\epsilon} \langle p p' | G_{cb}[W]. \quad (5)$$

The interaction parameters are chosen to reproduce the scattering phase shifts. Nucleonic three-body forces are included in order to (slightly) shift the saturation point of purely nucleonic matter to the empirical value.

For the quark phase, we use the MIT bag model with massless u and d quarks and massive s quark with $m_s = 150 \text{ MeV}$. The energy density ϵ_Q consists of the kinetic term by the Thomas-Fermi approximation, the leading-order one-gluon-exchange term⁷ proportional to the QCD fine structure constant α_s , and the bag constant B . Here we use $B = 100 \text{ MeV/fm}^3$ and $\alpha_s = 0$ to get the quark EOS which crosses the hadronic one at an appropriate baryon density.

3. Hadron-Quark Mixed Phase

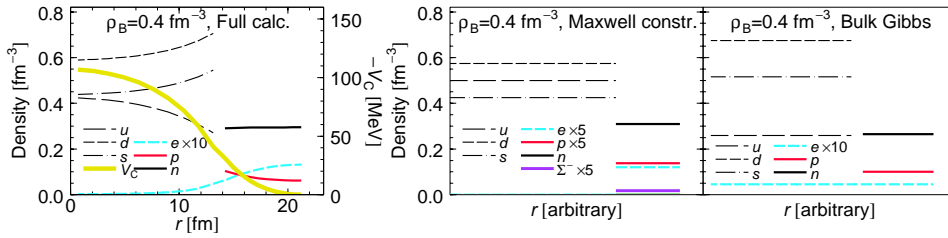


Fig. 1. Left: Density profiles and Coulomb potential V_C within a 3D (quark droplet) Wigner-Seitz cell of the MP at $\rho_B = 0.4 \text{ fm}^{-3}$. The cell radius and the droplet radius are $R_W = 26.7 \text{ fm}$ and $R = 17.3 \text{ fm}$, respectively. Center: Same as the left panel for MC case. The radius r is in arbitrary unit since there is no specific size. Right: The case of BG calculation.

Figure 1 illustrates an example of the density profile in a 3D cell. One can see the non-uniform density distribution of each particle species together with the

finite Coulomb potential; charged particle distributions are rearranged to screen the Coulomb potential. The quark phase is negatively charged, so that d and s quarks are repelled to the phase boundary, while u quarks gather at the center. The protons in the hadron phase are attracted by the negatively charged quark phase, while the electrons are localized to the hadron phase. This density rearrangement of charged particles causes the screening of the Coulomb interaction between phases.

In the center and right panels, compared are the cases of MC and BG. MC assumes the local charge neutrality, while the BG does not. One can see that the local charge neutrality in the full calculation lies between two cases. The localization of electrons which is one of the charge screening effects, reduces the local charge density. But the local charge density remains still finite to some extent.

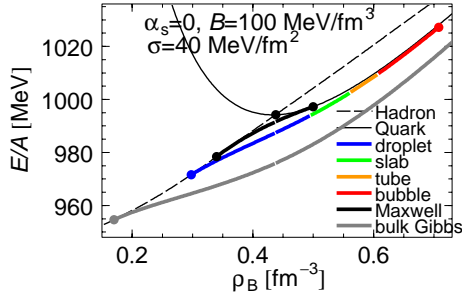


Fig. 2. EOS of the MP (thick curves) in comparison with pure hadron and quark phases (thin curves). hadron ($\rho_B < 0.44 \text{ fm}^{-3}$) or quark ($\rho_B > 0.44 \text{ fm}^{-3}$) phases. Each segment of the MP is chosen by minimizing the energy.

Figure 2 compares the resulting EOS with that of the pure hadron and quark phases. The thick black curve indicates the case of the MC, while the colored lines indicate the MP in its various geometric realizations starting with a quark droplet structure and terminating with a bubble structure. Note that the charge screening effect always tends to make matter locally charge neutral to save the Coulomb interaction energy. Hence, combined with the surface tension, it makes the non-uniform structures mechanically less stable and limits the density region of the MP.³ Consequently the energy of the MP is only slightly lower than that of the MC.

However, the structure and the composition of the MP are very different from those of the MC, which is demonstrated in Fig. 3, where we compare the particle fractions as a function of baryon density in the full calculation (left panel) and the MC (right panel). One can see that the compositions are very different in two cases. In particular, a relevant hyperon (Σ^-) fraction is only present in the MC.

The suppression of hyperon mixture in the MP is due to the absence of the charge-neutrality condition in each phase. As shown in Fig. 4, hyperons (Σ^-) appear in charge-neutral hadronic matter at low density (0.34 fm^{-3}) to reduce the Fermi energies of electron and neutron. Without the charge-neutrality condition,

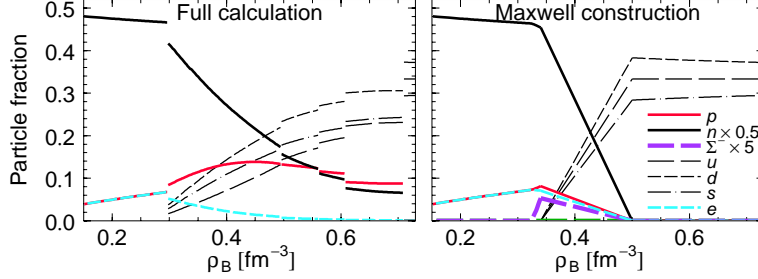


Fig. 3. Particle fractions in the MP by the full calculation (left panel) and the MC (right panel).

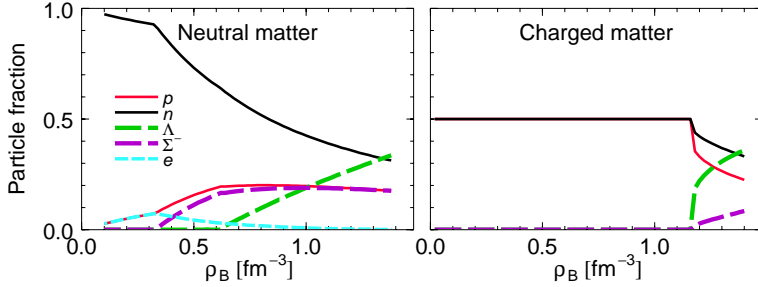


Fig. 4. Upper panel: Particle fractions of neutral matter with electrons (corresponding to neutron star matter). Lower panel: The same quantity for charged matter without electrons, the low-density part of which corresponds to symmetric nuclear matter. Both cases require chemical-equilibrium condition.

on the other hand, there appears symmetric nuclear matter at lower density and hyperons will be mixed above 1.15 fm^{-3} due to the large hyperon masses. The MP has positively charged hadron phase and negative quark phase though the Coulomb screening effect diminishes the local charge density. This brings the feature of symmetric nuclear matter into the hadron phase and, consequently, the mixture of hyperons is suppressed.⁸

4. Neutron Star Structure

Having the EOS comprising hadronic, mixed, and quark phase in the form $P(\epsilon)$, the equilibrium configurations of static NS are obtained in the standard way by solving the Tolman-Oppenheimer-Volkoff (TOV) equations⁹ for the pressure $P(r)$ and the enclosed mass $m(r)$,

$$\frac{dP}{dr} = -\frac{Gm\epsilon}{r^2} \frac{(1 + P/\epsilon)(1 + 4\pi r^3 P/m)}{1 - 2Gm/r}, \quad (6)$$

$$\frac{dm}{dr} = 4\pi r^2 \epsilon, \quad (7)$$

being G the gravitational constant. Starting with a central mass density $\epsilon(r=0) \equiv \epsilon_c$, one integrates out until the surface density equals the one of iron. This gives the

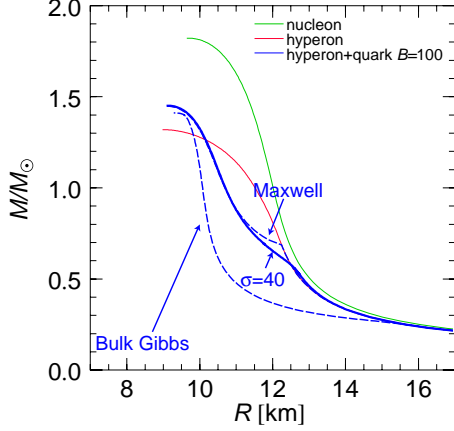


Fig. 5. (Color online) Neutron star mass-radius relations for different EOS and three different hadron-quark phase transition constructions. For the hybrid stars (blue and black curves), the dashed lines indicate the Maxwell (upper curves) or bulk Gibbs (lower curves) constructions and the solid lines the mixed phase of the full calculation.

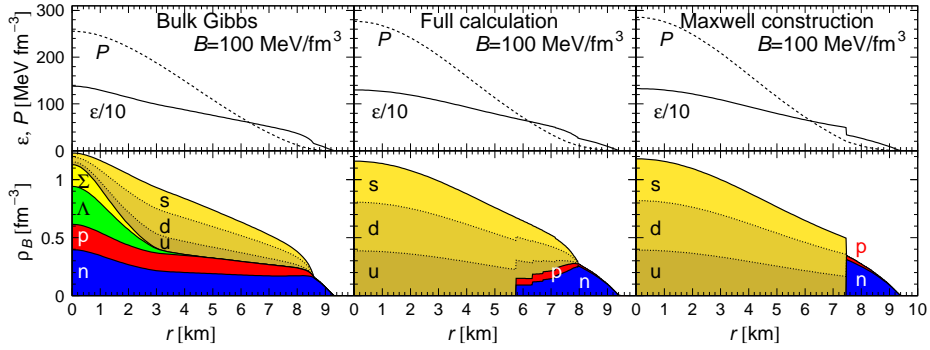


Fig. 6. (Color online) Internal structure of a $1.4 M_{\odot}$ neutron star obtained with three different phase transition constructions. The upper panels show total energy density and pressure and the lower panels the overall particle fractions as functions of the radial coordinate of the star, using the bulk Gibbs calculation (left panel), the mixed phase of the full calculation with $\sigma = 40 \text{ MeV}/\text{fm}^2$ (central panel), and the Maxwell construction (right panel). In all cases $\alpha_s = 0$ and $B = 100 \text{ MeV}/\text{fm}^{-3}$ are used.

stellar radius R and its gravitational mass $M = m(R)$. For the description of the NS crust, we have joined the hadronic EOS with the ones by Negele and Vautherin¹⁰ in the medium-density regime, and the ones by Feynman-Metropolis-Teller¹¹ and Baym-Pethick-Sutherland¹² for the outer crust.

Fig. 5 compares the mass-radius relations obtained with the different models. The purely nucleonic EOS (green curve) yields a maximum NS mass of about $1.82 M_{\odot}$, which is reduced to $1.32 M_{\odot}$ when allowing for the presence of hyperons (red curve). This feature has been shown to be fairly independent of the nucleonic

and hyperonic EOS that are used.¹³ The canonical NS with mass of about $1.4 M_{\odot}$ can therefore not be purely hadronic stars in our approach. In fact, the inclusion of quark matter augments the maximum mass of hybrid stars to about $1.5 M_{\odot}$:

In general, the Maxwell construction leads to a kink in the $M(R)$ relation, because the transition from a hadronic to a hybrid star occurs suddenly, involving a discontinuous increase of the central density when the quark phase onsets in the core of a star. The bulk Gibbs calculation yields smooth mass-radius relations involving a continuous transition from a hadronic to a hybrid star beginning at rather low central density corresponding to very low NS mass.

The MP construction by the full calculation lies between the two extreme cases, and with our choice of $\sigma = 40 \text{ MeV/fm}^2$ it is rather close to the Maxwell construction, smoothing out the kink of the hadron-hybrid star transition. This transition occurs generally at a fairly low NS mass, even below the natural minimum mass limit due to the formation via a protonneutron star¹⁴ and is thus an unobservable feature.

Whereas the maximum masses are practically independent of the phase transition construction, there are evidently large differences for the internal composition of the star. This is illustrated in Fig. 6 which show the total energy density, pressure, and particle fractions as a function of the radial coordinate for a $1.4 M_{\odot}$ NS. One observes with the bulk Gibbs construction (left panels) a coexistence of hadrons and quarks in a significant range of the star, whereas with the MC (right panels) an abrupt transition involving a discontinuous jump of energy and baryon density occurs at a distance $r \approx 7.5 \text{ km}$ from the center of the star. The small contamination with Σ^- hyperons in the hadronic phase is not visible on the scale chosen. The MP with the full calculation (central panels) lie between the two extreme cases, hadrons and quarks coexisting in a smaller range than in the bulk Gibbs cases.

5. Summary

In this article we have studied the properties of the mixed phase in the quark deconfinement transition in hyperonic matter, and their influence on compact star structure. The hyperonic EOS given by the BHF approach with realistic hadronic interactions is so soft that the transition density becomes very low if one uses the MIT bag model for the quark EOS.

The hyperon-quark mixed phase was consistently treated with the basic thermodynamical requirement due to the Gibbs conditions. We have seen that the resultant EOS is little different from the one given by the Maxwell construction. This is because the finite-size effects, the surface tension, and the Coulomb interaction tend to diminish the available density region through the mechanical instability, as has also been suggested in previous articles.^{15,16}

For the bulk properties of compact stars, such as mass or radius, our EOS gives similar results as those given by the Maxwell construction. The maximum mass of a hybrid star is around $1.5 M_{\odot}$, larger than that of the purely hyperonic star,

$\approx 1.3 M_{\odot}$. Hence we may conclude that a hybrid star is still consistent with the canonical NS mass of $1.4 M_{\odot}$, while the masses of purely hyperonic stars lie below it.

On the other hand, the internal structure of the mixed phase is very different; e.g., the charge density as well as the baryon number density are nonuniform in the mixed phase. We have also seen that the hyperon number fraction is suppressed in the mixed phase due to the relaxation of the charge-neutrality condition, while it is always finite in the Maxwell construction. This has important consequences for the elementary processes inside compact stars. For example, coherent scattering of neutrinos off lumps in the mixed phase may enhance the neutrino opacity.¹⁷ Also, the absence of hyperons prevents a fast cooling mechanism by way of the hyperon Urca processes.¹⁸ These results directly modify the thermal evolution of compact stars.

References

1. M. Baldo, G. F. Burgio, and H.-J. Schulze, *Phys. Rev. C* **58**, 3688 (1998); *Phys. Rev. C* **61**, 055801 (2000).
2. M. Baldo, G. F. Burgio and H.-J. Schulze, *Phys. Rev. C* **61**, 055801 (2000); O.E. Nicotra, M. Baldo, G.F. Burgio and H.-J. Schulze, *A & A* **451**, 213 (2006).
3. For a review, T. Maruyama, T. Tatsumi, T. Endo and S. Chiba, *Recent Res. Devel. Phys.* **7**, 1 (2006).
4. N. K. Glendenning, *Phys. Rev. D* **46**, 1274 (1992); *Phys. Rep.* **342**, 393 (2001).
5. T. Endo, T. Maruyama, S. Chiba and T. Tatsumi, *Prog. Theor. Phys.* **115**, 337 (2006).
6. T. Maruyama, T. Tatsumi, D. N. Voskresensky, T. Tanigawa and S. Chiba, *Phys. Rev. C* **73**, 035802 (2006).
7. E. Farhi and R. L. Jaffe, *Phys. Rev. D* **30**, 2379 (1984); M. S. Berger and R. L. Jaffe, *Phys. Rev. C* **35**, 213 (1987).
8. T. Maruyama, S. Chiba, H.-J. Schulze and T. Tatsumi, *Phys. Lett. B*, inpress; *Phys. Rev. D*, inpress.
9. S. L. Shapiro and S. A. Teukolsky, *Black Holes, White Dwarfs and Neutron Stars* (Wiley, New York, 1983).
10. J. W. Negele and D. Vautherin, *Nucl. Phys.* **A207**, 298 (1973).
11. R. P. Feynman, N. Metropolis, and E. Teller, *Phys. Rev.* **75**, 1561 (1949).
12. G. Baym, C. Pethick, and P. Sutherland, *Astrophys. J.* **170**, 299 (1971).
13. H.-J. Schulze, A. Polls, A. Ramos, and I. Vidaña, *Phys. Rev. C* **73**, 058801 (2006).
14. O. E. Nicotra, M. Baldo, G. F. Burgio, and H.-J. Schulze, *Astron. Astrophys.* **451**, 213 (2006); *Phys. Rev. D* **74**, 123001 (2006).
15. D. N. Voskresensky, M. Yasuhira, and T. Tatsumi, *Phys. Lett. B* **541**, 93 (2002); D. N. Voskresensky, M. Yasuhira, and T. Tatsumi, *Nucl. Phys.* **A723**, 291 (2003).
16. T. Tatsumi, M. Yasuhira, and D. N. Voskresensky, *Nucl. Phys.* **A718**, 359 (2003); T. Endo, T. Maruyama, S. Chiba, and T. Tatsumi, *Nucl. Phys.* **A749**, 333 (2005);
17. S. Reddy, G. Bertsch, and M. Prakash, *Phys. Lett. B* **475**, 1 (2000).
18. M. Prakash, M. Prakash, J. M. Lattimer, and C. J. Pethick, *Astrophys. J.* **390**, L77 (1992); T. Tatsumi, T. Takatsuka, and R. Tamagaki, *Prog. Theor. Phys.* **110**, 179 (2003); T. Takatsuka, S. Nishizaki, Y. Yamamoto, and R. Tamagaki, *Prog. Theor. Phys.* **115**, in press (2007).